Materials Science in Semiconductor Processing 168 (2023) 107839

Contents lists available at ScienceDirect

Materials Science in Semiconductor Processing

journal homepage: www.elsevier.com/locate/mssp

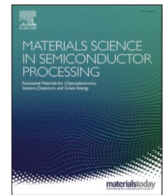

Pulsed 193 nm Excimer laser processing of 4H–SiC (0001) wafers with radiant exposure dependent *in situ* reflectivity studies for process optimization

A.P. Menduiña [a,b], A.F. Doval [b], R. Delmdahl [c], E. Martin [d,e], K. Kant [f], J.L. Alonso-Gómez [a,g], S. Chiussi [a,b,*]

[a] *CINTECX, Universidade de Vigo, New Materials Group, Vigo, 36310, Spain*
[b] *Applied Physics Department, Universidade de Vigo, E.E.I., Vigo, 36310, Spain*
[c] *Coherent LaserSystems GmbH & Co. KG, Göttingen, 37079, Germany*
[d] *IFCAE, Research Institute of Physics and Aerospace Science, Universidade de Vigo, Ourense, 32004, Spain*
[e] *Department of Mechanical Engineering, Heat Engines and Fluid Mechanics, Universidade de Vigo, E.E.I., Vigo, 36310, Spain*
[f] *CINBIO, Universidade de Vigo, Vigo, 36310, Spain*
[g] *Organic Chemistry Department, Universidade de Vigo, Vigo, 36310, Spain*

ARTICLE INFO

Keywords:
UV-Excimer laser
193 nm laser processing
Time Resolved Reflectivity
Silicon carbide
Graphene
Numerical simulation

ABSTRACT

193 nm Excimer lasers are efficient tools to process group-IV semiconductors for advanced microelectronic and photonic devices through crystallization annealing, or strain engineering. The combination of both, high photon energy and low penetration depth of the 193 nm laser pulses allow breaking most covalent bonds with a single photon, and low thermal budget treatments through a precise control of the laser processed volume. Up to now, studies using 193 nm lasers for silicon carbide (SiC) processing are mostly limited to ablation processes for micromachining purposes. This paper presents a first study to demonstrate that the optimization of other processes, like the creation or annealing of vacancies, the alloying of SiC surfaces or the selective ablation of silicon or carbon should also be feasible. To develop such laser assisted processes and optimize process parameters, a numerical simulation of the laser/material interaction is essential. This implies that the temporal evolution of the laser pulse must be well known, and that an "*in-situ* measurement" of the response of the material to the laser pulse should be available. This study therefore evaluates the temporal profile of a new high-power Excimer laser, and presents the results of *in-situ* Time Resolved Reflectivity (TRR) measurements obtained when irradiating 4H–SiC(0001) wafers with radiant exposures ranging from 0,1 J/cm^2 to 3,0 J/cm^2. The temporal pulse profile is determined, fitted and applied in a 1-D numerical simulation of the temperature gradients for Si(100) as reference sample, to validate the experimental findings. Radiant exposure thresholds at around 1,4 J/cm^2 to locally produce molten surfaces and 1,8 J/cm^2 to ablate and create carbon-rich regions with graphene, are determined *in-situ* and confirmed by Raman spectroscopy.

1. Introduction

Local processing of silicon carbide (SiC) substrates is of significant relevance to produce high-end electronic devices. Among the different SiC polytypes, the 4H hexagonal SiC with (0001) orientation, 4H–SiC (0001), is considered as the substrate material of choice for power electronic devices that need to operate at elevated temperatures with high frequencies [1,2].

For group-IV semiconductors based on silicon (Si) and germanium (Ge), we already presented several studies demonstrating that 193 nm Excimer lasers are highly efficient tools to produce, crystallize and anneal them, or to achieve dopant activation as well as strain engineering through epitaxial alloys. These lasers were also used to develop epitaxial alloys with other group-IV elements like tin (Sn), which paved the way to a new generation of microelectronic and photonic devices [3–8].

The advantage of using short 193 nm laser pulses of few tenth of nanoseconds duration, is that most covalent bonds can be broken with a

* Corresponding author. CINTECX, Universidade de Vigo, New Materials Group, Vigo, 36310, Spain.
E-mail address: schiussi@uvigo.gal (S. Chiussi).

https://doi.org/10.1016/j.mssp.2023.107839
Received 16 June 2023; Received in revised form 5 September 2023; Accepted 6 September 2023
Available online 14 September 2023
1369-8001/© 2023 The Authors. Published by Elsevier Ltd. This is an open access article under the CC BY license (http://creativecommons.org/licenses/by/4.0/).

single photon due the high photon energy of 6,4 eV, and that low thermal budget processes can be achieved by a fine control of the laser processed volume through precise confinement of the heated zones. Although conventional thermal treatment as well as laser processing of SiC substrates is widely studied, there are only few reports on 193 nm laser processing and most of them are limited to ablation processes for micromachining purposes [9,10].

To our best knowledge, 193 nm laser studies that aim the formation and annealing of colour centres and vacancies for "device-friendly" optically readable qubits in quantum electronics or in quantum spintronics, or the alloying of SiC surfaces with metals to create silicides and enhance the SiC/electrode interface, or the element separation to obtain highly conducting graphene patterns on a SiC substrate, are very rare.

For the control of vacancies, conventional thermal annealing is usually employed to stabilize them, remove interstitial related defects, or reduce the number of vacancies that are typically produced by electron or ion bombardment [11–13]. Only ultra-short laser pulses in the femtosecond regime were used to locally produce vacancies through laser processing, but not 193 nm Excimer lasers, yet [14,15].

In contrast, to enhance SiC/electrode contacts, which are usually improved by forming silicide and removing carbon residuals through thermal treatments, also 193 nm laser processing has already been proposed. A study of Lin et al., in 2019 indicates that the formation of an interfacial graphene layer between SiC wafer and gold (Au) contacts through only three 193 nm laser pulses of 2 J/cm^2 laser fluence, results in an improvement of the contact properties [16]. Later, in 2020, they also studied C-vacancies and distortions in laser-generated graphene for lower fluences and higher number of pulses [17].

As for producing graphene on SiC, the currently most efficient way to obtain carbon rich structures like graphene on SiC is the sublimation of Si in SiC wafer surfaces through conventional thermal treatments at 1000 °C–1600 °C, resulting in a reorganization of the residual carbon to graphite or graphene layers [18–20].

Some few studies using Excimer lasers were published [9,16,17,21–23], but to our best knowledge only one publication on micromachining used 193 nm radiation and reported graphene features in the heat affected zones (HAZs) [10]. Others aiming at surface improvements of SiC ceramics or laser cleaning of cubic, so called, β-SiC did not find any graphitization [24,25].

The reason that 193 nm Excimer lasers are still not established for these processes and that the reported experimental parameters largely vary and are sometimes contradictory, can be attributed to the higher heat resistance and optical penetration depth of SiC, compared to Si and Ge. This implies that high and stable laser pulse energies are crucial, particularly if large areas must be processed, as in semiconductor fabrication lines. Until now, this was a major issue when using conventional commercial 193 nm Excimer lasers, but with the development of the new LEAP laser generation, the Excimer laser performance has been strongly improved. The LEAP laser platform contains an innovative discharge design with capacitively coupled pre-ionization in conjunction with a solid-state switching module. The result is an improvement close to factor three of the pulse energy stability, even for high pulse energies and repetition rates. Moreover, the extended laser maintenance intervals, compared to previous laser generations, lead to significantly reduced unit costs in high volume processing. As a matter of fact, the LEAP laser has recently become a "workhorse" in three-shift, ablative thin film processing for semiconductor manufacturing [26].

Although the nominal pulse duration for the laser is provided by the manufacturer, a detailed study of its time evolution is needed as input for numerical simulations of the time dependent temperature profiles. Such numerical simulations are an ideal tool to understand the processes and to optimize relevant laser parameters, such as applied radiant exposure (H_e), which is often called fluence or energy density, and number of consecutive pulses, as typically done for SiGe processing [3,27].

Once the time dependent pulse profile is measured and either used numerically or fitted to be used in a simulation process, experimental feedback is needed to corroborate the simulated temperature profiles. This is often done combining several expensive and destructive techniques, like cross section High Resolution Transmission Electron Microscope (HR-TEM) and Time of Flight Secondary Ion Spectrometry (Tof-SIMS), among others [5]. A more economic and immediate "*in-situ* technique" to estimate the melting and ablation thresholds is monitoring the Time Resolved Reflectivity (TRR), i.e. changes in surface reflectivity during and after the 193 nm laser pulses. To quickly evaluate changes in composition and structure of the crystalline substrates, Raman spectroscopy is an adequate technique since it is non-destructive and, if probe lasers with short wavelength are used, also relatively shallow surface regions can be evaluated, as described in previous papers on laser processing of Si(100) based semiconductors [3–7].

This study focusses therefore on the first accurate evaluation of the 193 nm LEAP laser pulses and on the "*in situ* TRR measurements" obtained when irradiating the Si-face of 4H–SiC(0001) wafers as a function of radiant exposure in the particularly wide range of 0,1 J/cm^2 to 3,0 J/cm^2 and using 10 to 1000 consecutive pulses at 1 Hz of a spatially homogenized laser beam. The aim is to present our first approach to evaluate the laser parameters for "soft annealing" needed to create and anneal vacancies, melting of the substrate surface to allow future alloying processes with metals or segregate the Si to obtain Carbon rich surface patterns. Results obtained irradiating Si(100) as reference samples are also presented, together with a first simple 1-D numerical simulation of the temperature profiles for Si(100) in order to compare them with the experimental findings.

2. Experimental

2.1. Experimental set-up and materials

The experiments were performed with a newly developed LEAP-60A, ArF-Excimer laser (Coherent, Inc.) under ISO-5 clean room conditions and the laser pulse energy Q_e was adjusted with an optical attenuator (Lasoptics Micrometer Attenuator 193 nm) and homogenized by a "fly-eye" dual lens array homogenizer (Exitech, EX–HS–700D) with 2 arrays of 4 × 6 cylindrical lenses each and a 180 mm condenser lens. The pulse energy was monitored *in-situ* with a commercial pyroelectric energy meter (PM-1) (Ophir Laserstar, PE50-DIF), after its previous calibration close to the sample. The temporal evolution of the laser pulse and the time dependent reflection of a 635 nm CW-laser (LOA-2 Newport) by the irradiated volume were monitored for TRR measurement using fast photodetectors (PD-1 and PD-2) and Picoscope (3205 and 3206) USB-Oscilloscopes.

As shown in Fig. 1 with the complete experimental set-up, Excimer laser and probe laser were impinging on the sample surface with an angle of 0° and 60°, respectively. The sample was located on a motorized XYZ-stage (3 Newport MFA-CC/SMC-100CC linear translation stages), controlled by a home-made software using LabView 8.6. PD-1 and PD-2 were fast photodetectors with 1 ns rise time and the contribution of the UV radiation in the amplified (Hamamatsu C6438-01) TRR signals detected by PD-2 was filtered by a long pass 620 nm filter (Hoya R62, Edmund Optics).

Silicon (100 ± 0,5°) wafer (Siegert wafer) were irradiated as reference samples, to check the effects on the reflectivity and compare them with results obtained irradiating a 4H–SiC (0001) wafer (FhG Erlangen) with 4° off axis deviation. All processes were performed in air (45% relative humidity) under ISO-5 Clean room condition. The wafers were previously cleaned through ultrasonic bath immersions in acetone and isopropyl alcohol (5 min each) and finally rinsed with deionized water 18,2 MΩ × cm (23 °C), followed by final drying under a 99,999% N_2 flow.

The TRR signals are the reflected 635 nm probe laser intensity variation due to effects of the 193 nm laser pulses. Their evaluation is done using Equation (1), and the intensity change of the 635 nm probe

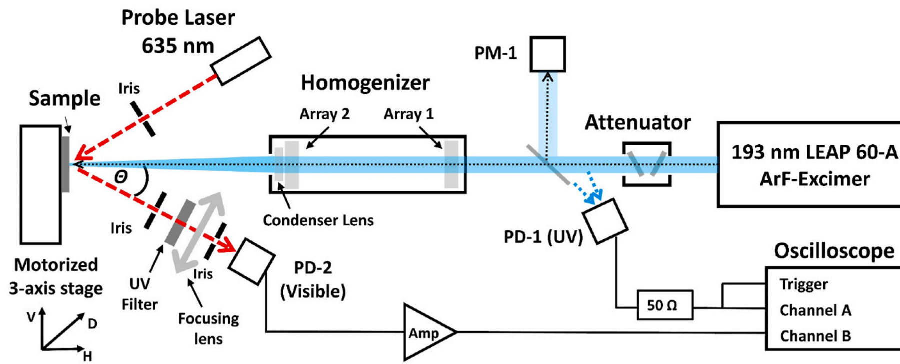

Fig. 1. Scheme of the experimental set-up.

laser is calculated as follows:

$$\Delta I_{\mathrm{R}}(\%) = 100\frac{(I - I_0 - I_{\mathrm{BG}})}{I_0 - I_{\mathrm{BG}}} \tag{1}$$

where I is the signal intensity due to the interaction of the material with the laser pulse, I_0 the intensity prior the pulse and I_{BG} the background signal with the Excimer pulse but without the probe laser. In addition, the TRR curves for the first three pulses were always discarded due to the possible alteration of the signal by evaporating impurities, humidity, or surface passivation layers.

In case of the widely studied Si(100), we calibrated the intensity values to obtain the change of reflectivity ΔR (%), according to the study of Diez et al. [28], considering the reflectivity of solid silicon $\mathrm{Si_{(s)}}$ and of fully molten silicon $\mathrm{Si_{(l)}}$ to be $R_{\mathrm{Si(s)}}$ = 34,8% and $R_{\mathrm{Si(l)}}$ = 71,2%, respectively. This procedure was not possible for the 4H–SiC(0001) due to lack of available data.

Raman spectra to determine changes in composition and structure were obtained using a Horiba Jobin Yvon LabRam HR800 spectrometer with 488,0 nm excitation laser at normal incidence, 100 × objective and 1800 lines grating. The laser power was kept at 0,67 mW to avoid additional heating effects induced by the Raman laser. Spectral calibration was performed using Ne (Oriel 6032) and Hg(Ar) (Oriel 6035) calibration lamps.

2.2. 193 nm Excimer laser

The beam characteristics of our LEAP-60A prototype (Coherent, Inc.) used for this study show Full Width at Half Maximum (FWHM) divergence angles of 1,0 mrad for the short and 3,6 mrad for the long axis of the laser beam cross section, and the deviation of the energy stability is of σ = 0,5%, according to the manufacturer when working at maximum repetition rate and pulse energy of 100 Hz and 400 mJ, respectively.

The radiant exposure H_{e} was calibrated by the ablation of commercial Cyclo Olefin Copolymer (COC) substrates (TOPAS 5013L, Advanced Polymers) below the saturation of the ablation rate and within a linear dependence of the ablation depth on the pulse energy Q_{e}. By evaluating the 3-D profile of the crater, we obtained the 3-D profile of H_{e} by multiplying Q_{e} with the ratio between the depth in a particular position and the total volume of the crater [29].

An example is shown in Fig. 2 with the 3-D profile plot for a laser pulse energy of Q_{e} = (13,7 ± 0,2) mJ, resulting in a highly uniform central top-hat area of approximately 1,0 mm × 2,5 mm.

The temporal irradiance profile $E_{\mathrm{e}}(t)$ of the 193 nm laser pulse has been characterized by recording the output voltage of a fast UV-sensitive photodiode working in photoconductive mode. The signal was digitized for a time of 500 ns, which is long enough for the irradiance to decay completely. The sampling interval was 1 ns. A set of 32 synchronized recordings was acquired and averaged for noise reduction.

Assuming that the photodiode voltage is proportional to the irradiance, the irradiance by radiant exposure temporal profile $E_{\mathrm{e}}(t)/H_{\mathrm{e}}$ (Fig. 3) is obtained by dividing the measured voltage signal by its integral (which is numerically evaluated). The temporal irradiance profile $E_{\mathrm{e}}(t)$ can be eventually calculated by multiplying by the local value of the radiant exposure H_{e}, obtained from the pulse energy Q_{e} as aforementioned. The FWHM of the pulse measured on this temporal profile is 20,6 ns.

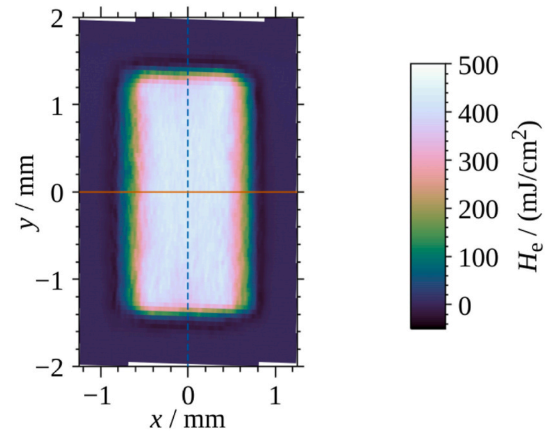

Fig. 2. 3-D radiant exposure profile of the laser spot for Q_{e} = (13,7 ± 0,2) mJ pulse energy.

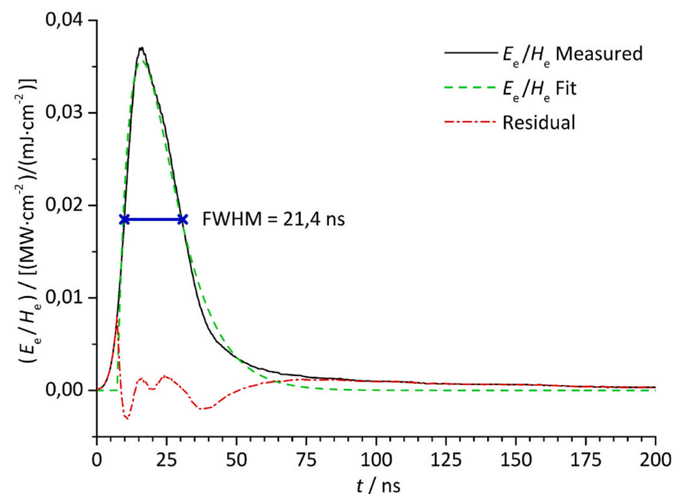

Fig. 3. Measured and fitted temporal pulse profile with evaluation of its error. Fitted FWHM is given in the graph.

2.3. 1-D numerical simulation

The numerical simulation of the time dependent temperature was obtained through 1-D unsteady simulations of the c-Si(100) heating process, based on the approach for describing the laser melting of crystalline Si by Unamuno et al. [30], and using the numerical software Comsol Multiphysics based on Finite Element Methods (FEM) as described in a previous paper [31]. The laser time profile $f(t)$ was normalized and integrated in the numerical model. The heat distribution in depth, treated as a source term in the 1-D heat transfer equation, was imposed as described in Equation (2).

$$Q_p = \frac{H_e}{\tau} f(t)(1-R)\frac{1}{\delta}\exp^{-x/\delta} \tag{2}$$

Here x stands for the depth of each point within the sample, H_e is the radiant exposure, and τ is the integral of the normalized pulse profile along the pulse time. Parameters for absorption length δ were taken as $\delta = 1/\alpha$ with α being the absorption coefficients, according to Unamuno et al. [30], while reflectance R for 193 nm at 300 K was taken from the final fit for the 3 eV–7 eV range published by in Green al. and estimated to be 69% [32].

3. Results and discussion

3.1. Laser pulse fit

Although the digitized profile has been used for the numerical simulations in this work, it is also interesting to have a reasonable fit of the LEAP-60A pulse to an analytical model thus being able to compare the experimental findings with those obtained in prior studies or with other laser models.

We used the model presented in Equation (3) of [31], that consists in the product of time by an exponential function and can be written as:

$$\frac{E_e(t)}{H_e} = \begin{cases} a\,t\,\exp\left(-\frac{t}{\tau}\right) & \text{for} \quad t \geq 0 \\ 0 & \text{for} \quad t < 0 \end{cases} \tag{3}$$

The measured profile was fitted to this function by using the Levenberg-Marquardt algorithm. The values of the fit parameters are $a = 0{,}0111$ MW/(mJ·ns) and $\tau = 8{,}75$ ns that, according to the properties of Equation (3), correspond to a FWHM of 21,4 ns. The resulting curve is also shown in Fig. 3. Both, the measured FWHM value of 20,6 ns and the fitted one of 21,4 ns, match well with the value of 22 ns provided by the manufacturer. The pulse profile itself is sharper that the ones known for the typical previous 193 nm Excimer laser generations, like the LPX 220i (Lambda Physik), since it shows a decay to roughly 10% of the maximum value after 50 ns, compared to 30% for the pulses of the previous laser [7].

3.2. 1-D numerical simulation

The numerical simulation of the temporal temperature evolution was done for some H_e values below and above the estimated melting threshold and plotted in Fig. 4.

According to the numerical simulations, the melting and vaporization/ablation thresholds using the LEAP-60A laser pulses should take place at H_e slightly below 0,60 J/cm^2 and well above 1,34 J/cm^2, respectively. A significant increase of the melt duration with increasing H_e can also be observed in the temperature profiles. Moreover, the simulation allows also to predict the maximum depth $d_{(max)}$, as well as the start $t_{(i)}$, end $t_{(end)}$, thus duration $\Delta t_{(melt)}$ of the molten pool, as summarized in Table 1.

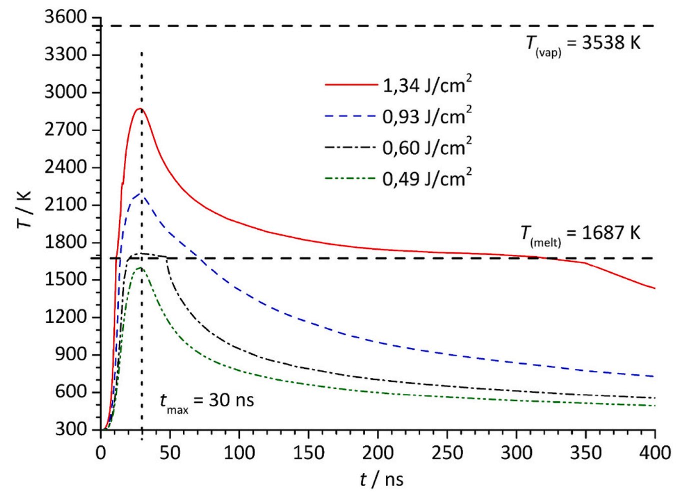

Fig. 4. Time dependence of the temperature at the sample surface for different H_e. Dashed horizontal lines show the melting and vaporization temperatures of Si(100) and the vertical one the approximate peak surface temperature.

Table 1
Maximum depth of molten pool, its start, and end with respect to the laser pulse onset, and molten pool duration.

H_e / J/cm^2	$d_{(max)}$ / nm	$t_{(i)}$ / ns	$t_{(end)}$ / ns	$\Delta t_{(melt)}$ / ns
0,48	0	0	0	0
0,60	27	19,6	53,5	33,9
0,93	305	14,2	70,3	50,7
1,34	863	11,1	313	301,9

3.3. TRR of the Si(100) reference sample

The TRR curves for three radiant exposures H_e leading to molten pools are plotted in Fig. 5. A first cross-check with the literature values indicates that the reflectivity of 38%–40% for the onset of melting silicon $Si_{(m)}$ is in reasonable agreement with the value of 39,8% published

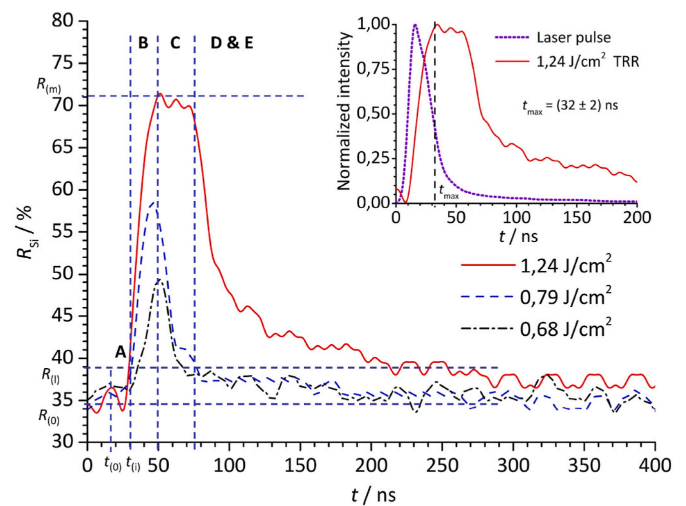

Fig. 5. TRR for three values of H_e producing molten pools with horizontal dashed lines for $R_{(0)}$, $R_{(l)}$, and $R_{(m)}$, the reflectivity of solid, melting and melted Si, respectively. Vertical dashed lines indicate instants for starting interaction with the 193 nm laser pulse $t_{(0)}$ and melting $t_{(i)}$, defining zones **A** and **B**. For $H_e = 1{,}24$ J/cm^2, heating and cooling of a molten pool depth beyond the 635 nm TRR sensitivity are marked, defining zones **C**, **D** and **E**. The inset shows laser pulse and TRR for $H_e = 1{,}24$ J/cm^2, starting at t_0.

by Diaz et al. [28]. However, other previous accurate studies on this topic provide a wide range of reflectivity values of around 34%–35%, 70%–73%, and of 41% for solid, liquid and melting silicon, respectively [33,34].

The experimental results are in reasonable agreement with the numerically simulated ones and the approximated instant of maximum temperature of 30 ns in Fig. 4 matches with the one at (32 ± 2) ns for maximum reflectivity of a fully molten pool (inset of Fig. 5), within its experimental error. The results for the highest H_e value of 1,24 J/cm^2, plotted in Fig. 5, clearly evidence regions that can be associated to heating of the solid **(A)**, melting and deepening of the molten pool **(B)**, molten volume that is deeper than the depth sensitivity of 635 nm TRR **(C)**, and its cooling **(D)** with the final cooling of the solid **(E)**.

If we evaluate the TRR spectra in terms of maximum reflectivity and melt duration for the different H_e, we obtain Figs. 6 and 7, showing the maximum reflectivity and the duration of the molten pool as function of H_e, respectively.

As shown in Fig. 6, again different regions can be defined and associated to the heating of the solid material **(1)**, its melting until reaching the depth where the sensitivity of the TRR measurement with a 635 nm laser falls to zero **(2)**, the heating and cooling of the molten pool beyond this depth **(3)**, and the ablation of the material **(4)**. This last region is showing apparently random reflectivity values due to the emission of an ablation plume with consequently shadowing of the probe laser and of the Excimer laser pulse tail, as well as the roughening of the surface. The graphically estimated threshold values for H_e are of around 0,5 J/cm^2 to 0,6 J/cm^2 and 1,5 J/cm^2 to 1,7 J/cm^2 to melt and ablate, respectively. By fitting data points to a curve that is based on a modified Weibull cumulative distribution function and considering as melting threshold a deviation of 5% from the tangent of the curve at the point of maximum slope, we obtain a melting threshold of H_e = 0,56 J/cm^2, that matches with the simulated values in Fig. 4 and Table 1.

On the other hand, by evaluating the time that the reflectivity is above 39% we obtained the radiant exposure dependent molten pool duration $\Delta t_{(melt)}$ for the 4th pulse in each experiment with different H_e values (Fig. 7), finding again a reasonable correlation with the numerically simulated values in Table 1 for the regions **(1)** and **(2)**. For region **(3)**, with a rather deep molten pool, the experimental data seem to underestimate the melt duration of the surface layer, compared to the simulated data. Region **(4)**, associated to ablation, shows now rather random values that are difficult to obtain because of relatively high measurement error in regions **(3)** and **(4)** (estimated about 10%), due to the fluctuation of the signal intensity. Averaging signals of several pulses

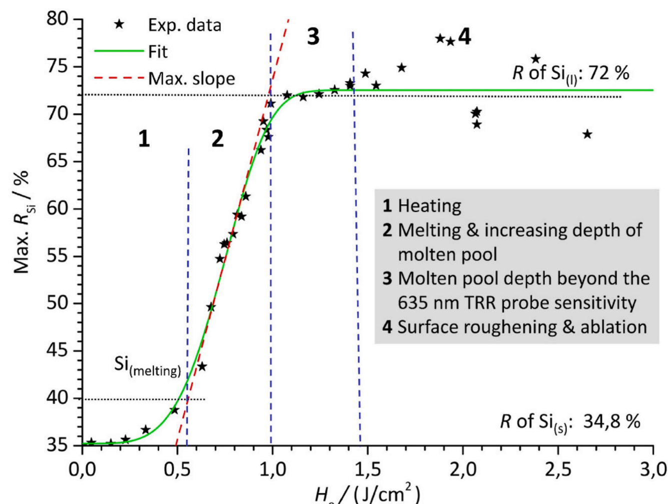

Fig. 6. Max. R_{Si} values as function of H_e with the ones for solid $Si_{(s)}$ and liquid $Si_{(l)}$. A fitted curve with its tangent of maximum slope is also plotted and regions **1** to **4** marked and explained.

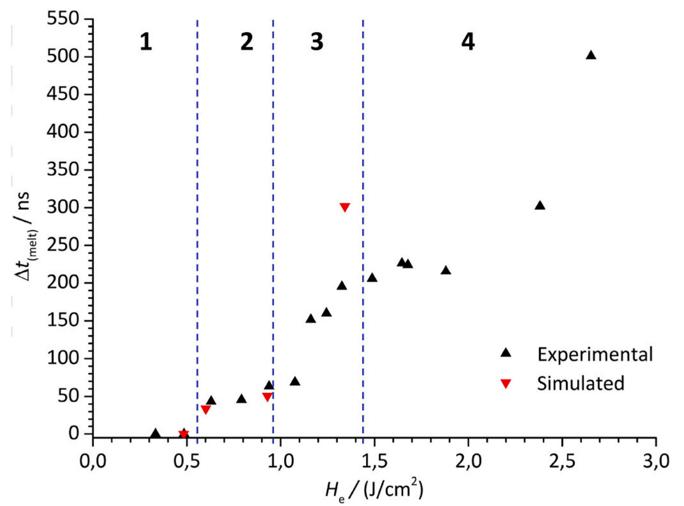

Fig. 7. Duration of molten pool Δt_{melt} for Si(100) as function of H_e. Regions defined in Fig. 6 are shown and simulated data from Table 1 are included.

and fitting the curves would greatly reduce the error, but care must be taken with changes of $\Delta t_{(melt)}$ due to possible modifications of the substrate surface composition, structure, and morphology during the laser treatment.

Nevertheless, the H_e threshold value for melting can now be easily determined by the intersection at $\Delta t_{melt} = 0$ ns and is at around 0,55 J/cm^2, while the threshold for fully molten pool withing the 635 nm TRR sensitivity, is at around 1,1 J/cm^2, in agreement with the previous findings.

The results show that with the high laser pulse energies of the new industrial LEAP platform, its relatively low FWHM and the use of an optical beam homogenizing system delivering large uniform spots, both an accurate "*in-situ* monitoring" through TRR as well as a 1-D numerical simulation of the process can be performed.

The excellent matching of H_e threshold values and of reflectivity as well as of the simulated temperature dependencies corroborate the reliability of these techniques to predict and optimize the radiant exposure values for H_e sensitive processes, as shown in previous studies [3–7].

3.4. TRR of the 4H–SiC(0001) sample

As explained in the experimental part, the lack of literature data about the temperature dependent reflectivity of 4H–SiC(0001) and its very low reflectivity for 635 nm at room temperature, made a calibration of the reflectivity values, as done for Si(100), unreliable. We therefore evaluated the changes in signal intensity, reflected by the polished irradiated Si face of the 4H–SiC wafer, according to Equation (1), equivalent to the change of reflectivity ΔR. Fig. 8 shows the TRR spectra obtained for representative radiant exposures, namely the H_e of 0,53 J/cm^2 without melting, of 1,33 J/cm^2 and 1,76 J/cm^2 with melting that show similar shapes as for Si(100), and of 2,28 J/cm^2 and 2,43 J/cm^2, where a second peak and a considerable decrease of the reflectivity with respect to the initial value can be observed.

Like for the Si(100) in Fig. 5, different regions can be identified and associated to the heating of solid **(A)**, to major changes due to amorphization and/or melting **(B)**, and a deepening of the molten pool **(C)**. But now, at H_e = 1,76 J/cm^2 and above, a second peak emerges (Fig. 8), that does not exist for the Si (Fig. 5). Moreover, the regions for cooling of liquid **(D)** and solid **(E)** are now accompanied by a strong decrease of the final reflectivity compared to the initial one, that can be attributed to surface roughening, either caused by segregation or ablation of Si, C or SiC.

Using the plateaus in the tail of the TRR curves, that correspond to

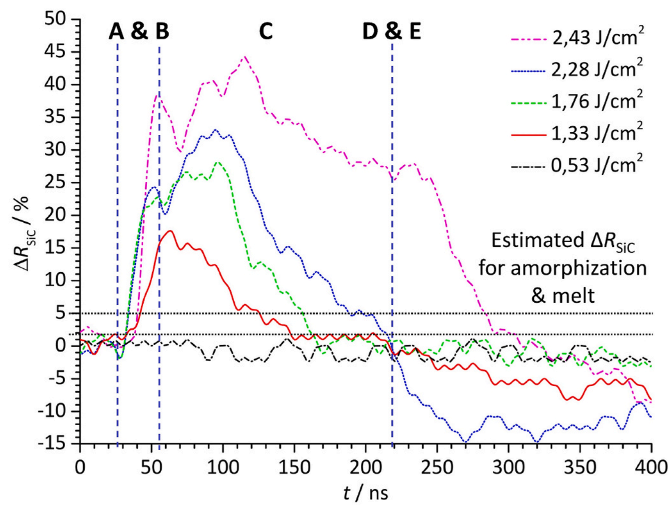

Fig. 8. Time dependent TRR measurements of SiC reflectivity changes ΔR for 5 different H_e values are plotted, and regions **A** to **E** are indicated. The horizontal dashed lines indicate the estimated range of ΔR values for the possible melting thresholds.

the reflectivity of a molten surface with an underlying molten volume that is slowly cooling down, we have estimated very roughly that the change in reflectivity for melting is between 2% and 5%.

Similar to the Si(100), we also analysed the maximum change in reflectivity as a function of the radiant exposure, plotted in Fig. 9 and estimated that the change in reflectivity associated to major compositional and/or structural changes through amorphization or melting, ΔR_{SiC}, is at around 5%.

A first region for H_e below 0,9 J/cm^2, approximately, does not evidenced any increase of reflectivity. However, since the photon energy of 193 nm is of 6,4 eV, thus high enough to induce photolytic processes in the SiC bonds with 4,6 eV bond energy and its bandgap of 3,26 eV [16, 35], we can consider that this experimental window could be adequate for "soft" UV treatments to produce colour centres or vacancies. With slightly higher radiant exposures an amorphization due to the formation of excessive defects is suggested and, once the surface apparently starts melting, at around 1,2 J/cm^2 to 1,3 J/cm^2, annealing and recrystallization or formation of silicide with metallic coatings can occur, as demonstrated in previous studies on SiGeSn alloys [4–7]. The observation of a second peak at radiant exposures above 1,76 J/cm^2, evidence that now drastic changes occur in the SiC or at least on its surface. Such a second peak has also been reported by Choi et al. but using a 308 nm Excimer laser with an apparently unique temporal profile showing three humps within around 150 ns, that has been associated to the formation of silicon and 3C–SiC layers [23]. Since this double peak appears also for our sharp laser pulse, it is most likely caused by a possible separation of the materials with the very different melting temperatures of 1689 K, 3103 K, and 4323 K for Si, SiC and C, respectively. Consequently, segregation and/or partial ablation should occur, with the reorganization to graphitic structures or graphene, as observed in other studies [10,16,17,23].

The evaluation of the roughly estimated melt duration, as done for the Si(100), but now taking $\Delta R_{SiC} = 5\%$ as reference for the melting threshold, is plotted in Fig. 10.

Our evaluation does not discriminate between the different elements, thus it can be assumed that the one with the lowest melting and resolidification temperature, the Si, will determine the total melt duration. According to this plot, the onset of melting and possible segregation is at radiant exposures of around 1,2 J/cm^2 to 1,3 J/cm^2, but a clear threshold for segregation is not detectable.

The obtained TRR results on 4H–SiC show that a large variety of processes can be *in-situ* monitored thanks to the very different reflectivity behaviour. A fine adjustment of the laser parameters should now allow to produce a "soft UV-treatment", annealing, thus the formation and curing of vacancies for quantum computing and spintronics, melting of a shallow surface region to alloy the SiC surface with metals and improve the properties of electrodes on SiC and phase separation to pattern Si or C features on the SiC wafer surfaces.

3.5. Raman spectra of irradiated 4H–SiC(0001)

In view of the previous results, we analysed the samples via non-destructive Raman spectroscopy using 488 nm excitation, to detect the effects of the 193 nm radiation on the 4H–SiC(0001) surface. Figs. 11 and 12 show the spectra of the original wafer and of spots treated with 100 pulses and H_e values below the melting threshold. No changes with respect to the original 4H–SiC (0001) wafer peaks, reported in the literature, can be observed, even when analysing the ratio between the peaks related to SiC lattice and SiC stacking faults [35–39]. The inset in Fig. 11 shows the region from 1000 cm^{-1} to 3200 cm^{-1} where graphitic structures, if present, should appear. The fact that the background of the spectra is increasing with H_e might be associated to the formation of

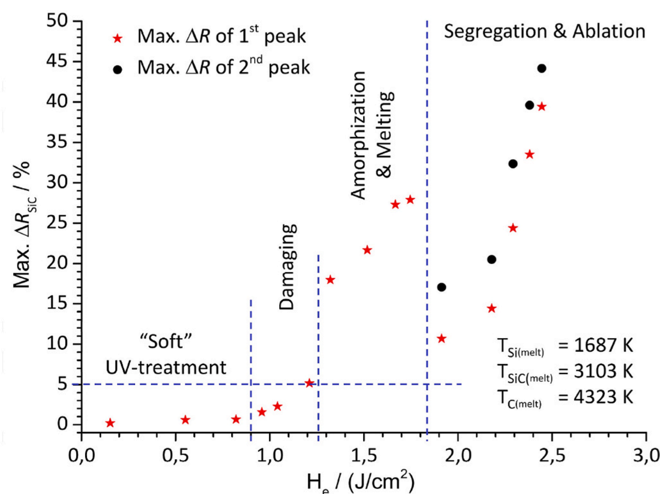

Fig. 9. Maximum change of R as function of H_e for both, the first and second peak. The horizontal dashed line indicates the estimated damage threshold and the vertical lines different possible processing windows. Melting temperatures for Si, SiC, and C are included as reminder.

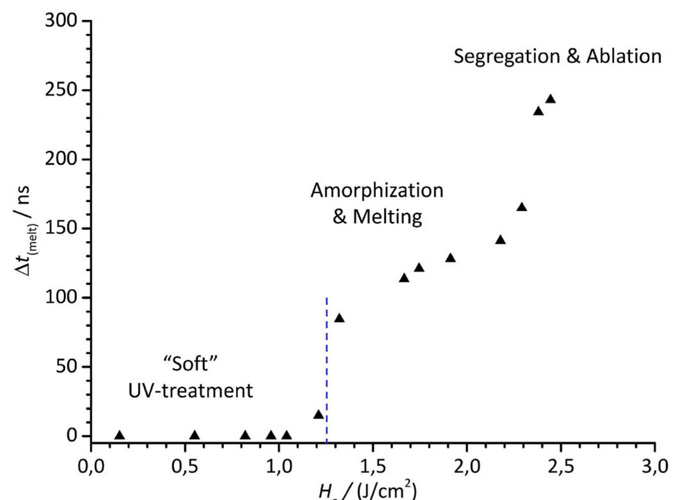

Fig. 10. Duration of molten pool in 4H–SiC as function of the radiant exposure. Onset of melting can be defined as the intersection of the plotted edge with the horizontal axis.

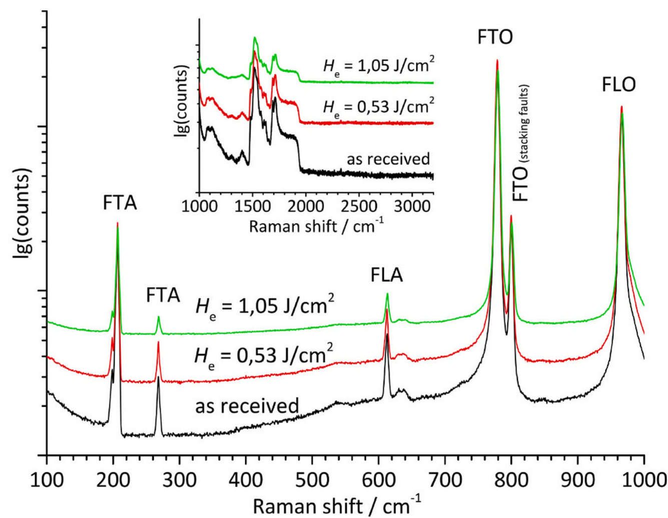

Fig. 11. Representative Raman spectra of SiC irradiated with 100 pulses and H_e values below the melting threshold, according to our TRR. Spectra are slightly stacked to allow their comparison. Assignment of the folded (F) SiC modes of transverse (T) or longitudinal (L), acoustic (A), and optic (O) branches was done according to reference data [35–39].

vacancies or defects, but a reliable corroboration of this assumption requires at least the use of other complementary techniques, like HR-TEM and Photoluminescence (PL) and is not the aim of this general contribution on 193 nm laser processing of SiC.

This behaviour changes dramatically when increasing the radiant exposure as shown in Fig. 12(a) and (b) evidencing clear bands associated to silicon and carbon, respectively. Particularly interesting is the fact that at $H_e = 1{,}52$ J/cm^2, a clear broad amorphous silicon (a-Si) band at around 480 cm^{-1} is accompanied by a crystalline silicon (c-Si) peak at a surprisingly high value of 523 cm^{-1}, usually associated to compressive strained Si. When the H_e value increases to 2,04 J/cm^2 and 2,54 J/cm^2 the intensity of the a-Si band vanishes and the c-Si peak position decreases to 518 cm^{-1}, indicating the presence of nano-crystalline silicon (nc-Si), as described by Kole et al. [39]. This c-Si peak shift to lower wavenumbers is associated to quantum confinement, as widely studied for nc-Si films and microcrystalline SiC films and can be used to evaluate both, its crystalline fraction and grain size [40–42]. However, a detailed study of the c-Si peak positions is not straightforward, because the interaction of the Si lattice with the one of the 4H–SiC wafers should lead to a rather complex strain behaviour that is usually only investigated for the growth of SiC on Si [38].

In the higher Raman shift spectral region, characteristic graphite, and graphene or nanographene features can be observed. As can be seen in Fig. 12(b), clear bands at around 1360 cm^{-1}, 1590 cm^{-1}, 2715 cm^{-1}, and 2933 cm^{-1} are evident. These four bands are typically associated to the so-called defect-induced D band, the in-plane vibrational G band, the 2 phonon D band, also called G′ band, and the D′ bands associated to disordered carbon structures, respectively [43–46].

An increase in radiant exposure leads apparently to more intense graphene bands due to a probably thicker graphene layer, but also to an increase of their disorder and the formation of so-called nano-graphene. An estimation of the number of layers and of the disorder, could be done by the evaluation of the G′ band, but the detailed characterization of the effects of stress, disorder, impurities, thickness etc. is beyond the scope of this general paper on 193 nm laser processing of SiC. Here we aim at demonstrating that graphitic structures, including graphene, are produced and that the intensity ratio of the peaks as well as their position are strongly influenced by the applied radiant exposure. The spectra presented in a detailed Raman study of epitaxial graphene (EG) on 6H–SiC(0001) produced by conventional thermal procedures, show almost identical features, being the one for $H_e = 1{,}52$ J/cm^2 similar to

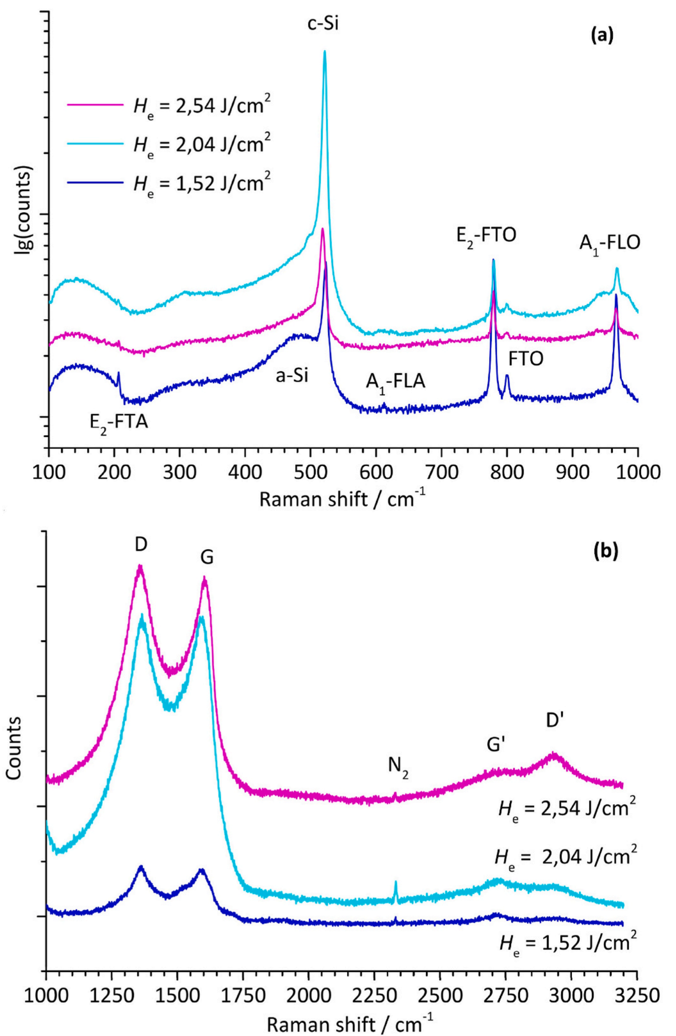

Fig. 12. Representative Raman spectra of samples irradiated with 100 pulses and values of H_e above the melting threshold, according to our TRR. Spectra are slightly stacked to allow their comparison. The emerging a-Si band and c-Si peak **(a)** as well as the D and G bands **(b)** associated to carbon and graphene are marked. A N_2 peak from air is also visible and serves as additional proof of the spectral calibration.

the EG on the Si face and the one for $H_e = 2{,}54$ J/cm^2 to the one for EG on the C-face of SiC [44].

It is also worth mentioning that the increase of H_e produces regions or islands with Si rich features that "free" carbon-rich regions in between. For recording the Raman spectra, these islands of several tens of microns size were avoided, since they only show c-Si features.

The effect of the number of pulses was finally also evaluated and plotted for the sample irradiated with $H_e = 1{,}52$ J/cm^2 using different number of consecutive pulses at 1 Hz. For this series, only the graphene related region is presented, where different shapes, intensity ratios and positions of the G′ and D′ bands can be observed when varying the number of pulses (Fig. 13).

When irradiating with only 10 pulses, the defect related band around 2950 cm^{-1} seems to be dominant, while 50 pulses lead to a predominant band around 2705 cm^{-1}, that could be associated to stressed epitaxial graphene (EP) on SiC [44]. Increasing the number of pulses shifts this band to higher values at around 2720 cm^{-1}, associated to larger number of graphene layers or stressed EP layers on SiC, but also leads again to the defect related band at 2950 cm^{-1}.

The Raman results corroborate that the laser processes, predicted analysing the TRR results, can be achieved with our industrial 193 nm

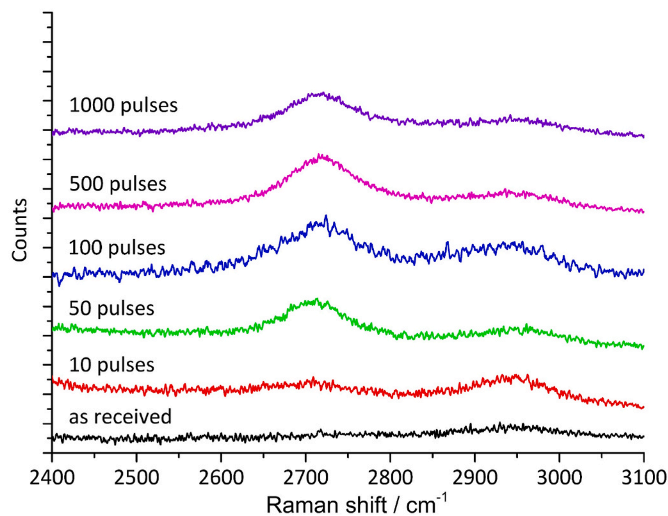

Fig. 13. Representative Raman spectra of samples irradiated with different number of pulses using H_e = 1,52 J/cm^2.

LEAP-60A Excimer laser. A fine control of the laser parameters can be provided by numerical simulation and "*in situ*" monitored by TRR measurements, thus opening a wide variety of interesting research fields using low, medium, and high H_e values. Creating and annealing vacancies, local melting of the SiC surface for silicide formation and phase separation to obtain graphene seem to be the most fascinating ones, together with local strain engineering of the SiC surface.

4. Conclusions

The first accurate evaluation of the laser pulse obtained by a novel industrial LEAP-60A ArF Excimer laser has shown that the measured and fitted FWHM of the pulse is of around 21 ns and that the lateral distribution of the radiant exposure can be accurately fine-tuned to values of up to 3,5 J/cm^2 for a highly uniform top-hat laser spot area of approximately 1,0 mm × 2,5 mm. The 1-D numerical simulations using the pulse characteristics of this new laser generation allowed the calculation of temporal and depth distributions of the temperature in Si(100), that match well with the corresponding "*in-situ* monitored" TRR results. The evaluation of both, the maximum reflectivity values and the melt duration allowed to determine the radiant exposure needed for different processes and their threshold values, like the melting threshold at H_e = 0,56 J/cm^2, thus validating the technique as a tool to optimize the laser processing parameters for this laser and for our experimental TRR setup.

Applying a similar procedure to 4H–SiC (0001) wafers and using a particularly wide range of radiant exposures from H_e = 0,1 J/cm^2 to H_e = 3,0 J/cm^2 at 1 Hz, evidenced H_e threshold values of 0,9 J/cm^2, 1,2 J/cm^2 and 1,7 J/cm for slight modification, amorphization with melting, and element segregation, respectively.

The 488 nm Raman analysis finally corroborated the experimental findings and indicated the formation of nc-Si and graphene with interesting dependencies of strain, number of layer and defects on both radiant exposure and number of pulses that were tested in a range of 10 to 1000 consecutive pulses. These results pave the way to well-controllable, high yield SiC processing for carbon rich surface patters on SiC wafer.

This paper presents therefore a first study to demonstrate that the optimization of different laser processes, like the creation or annealing of vacancies, the alloying of molten SiC surfaces with other materials or the selective ablation of silicon or carbon should be feasible. As a result of this first evaluation, narrower experimental windows for the 193 nm laser processes can now be studied, aiming the creation, and annealing of vacancies for quantum electronics and spintronics, the melting of metals with shallow SiC surface regions to improve electrical contacts, and the production of specific carbon rich surface patterns on SiC for new device concepts.

CRediT authorship contribution statement

A.P. Menduiña: Investigation, Data curation, Writing – original draft. **A.F. Doval:** Methodology, Formal analysis, Data curation, Conceptualization. **R. Delmdahl:** Writing – review & editing, Visualization. **E. Martin:** Investigation, Data curation, Conceptualization. **K. Kant:** Writing – review & editing, Investigation. **J.L. Alonso-Gómez:** Writing – review & editing, Funding acquisition. **S. Chiussi:** Supervision, Methodology, Funding acquisition, Data curation, Conceptualization, Writing – review & editing.

Declaration of competing interest

The authors declare that they have no known competing financial interests or personal relationships that could have appeared to influence the work reported in this paper.

Data availability

Data will be made available on request.

Acknowledgements

We greatly acknowledge the iisb-Fraunhofer and LEB-FAU members J. Schulze, T. Erlbacher, J. Schwarberg, and C. Gobert for the 4H–SiC (0001) wafer and for helpful discussions, as well as P. Barbazan, T. Padín and C. Serra from CACTI-UVigo for the 3-D profiler measurements, E. López CACTI-UVigo for sharing the HR-Raman spectrometer, and F. Poza for advising students during the development of the used LabView based software. Financial support was provided by Xunta de Galicia (ED431C-2021/49) and MICINN-Spain (TED2021-131760B–I00). K. Kant acknowledges support by the European Union Horizon 2020 research and innovation program under the Marie Sklodowska-Curie grant agreement 894227.

References

[1] C. Langpoklakpam, A.C. Liu, K.H. Chu, L.H. Hsu, W.C. Lee, S.C. Chen, C.W. Sun, M. H. Shih, K.Y. Lee, H.C. Kuo, Crystals 12 (2022) 245, https://doi.org/10.3390/cryst12020245.
[2] H. Matsunami, Proc. Jpn. Acad. B 96 (2020) 235, https://doi.org/10.2183/pjab.96.018.
[3] S. Chiussi, P. González, J. Serra, B. León, M. Pérez-Amor, Appl. Surf. Sci. 106 (1996) 75, https://doi.org/10.1016/S0169-4332(96)00441-2.
[4] S. Chiussi, C. Serra, J. Serra, P. González, B. León, S. Urban, G. Andrä, J. Bergmann, F. Falk, F. Fabbri, L. Fornarini, S. Martelli, F. Rinaldi, Appl. Surf. Sci. 186 (2002) 166, https://doi.org/10.1016/S0169-4332(01)00614-6.
[5] S. Chiussi, F. Gontad, R. Rodríguez, C. Serra, J. Serra, B. León, T. Sulima, L. Höllt, I. Eisele, Appl. Surf. Sci. 254 (2008) 6030, https://doi.org/10.1016/j.apsusc.2008.02.183.
[6] S. Stefanov, J.C. Conde, A. Benedetti, C. Serra, J. Werner, A.M. Oehme, J. Schulze, D. Buca, B. Holländer, S. Mantl, S. Chiussi, Appl. Phys. Lett. 100 (2012), 104101, https://doi.org/10.1063/1.3692175.
[7] S. Stefanov, J.C. Conde, A. Benedetti, C. Serra, J. Werner, M. Oehme, J. Schulze, S. Chiussi, Thin Solid Films 520 (2012) 3262, https://doi.org/10.1016/j.tsf.2011.10.101.
[8] S. Wirths, R. Geiger, N. von den Driesch, G. Mussler, T. Stoica, S. Mantl, Z. Ikonic, M. Luysberg, S. Chiussi, J.M. Hartmann, H. Sigg, J. Faist, D. Buca, D. Grützmacher, Nat. Photonics 9 (2015) 88, https://doi.org/10.1038/nphoton.2014.321.
[9] B. Pecholt, S. Gupta, P. Molian, J. Laser Appl. 23 (2011), 012008, https://doi.org/10.2351/1.3562522.
[10] A.F. Mohammed, Q.A. Al-Jarwany, A.J. Clarke, T.M. Amarald, J. Lawrence, N. T. Kemp, C.D. Walton, Chem. Phys. Lett. 713 (2018) 194, https://doi.org/10.1016/j.cplett.2018.09.057.
[11] S. Castelletto, A. Boretti, J. Phys.: Photon. 2 (2020), 022001, https://doi.org/10.1088/2515-7647/ab77a2.
[12] R. Nagy, M. Niethammer, M. Widmann, Y.C. Chen, P. Udvarhelyi, C. Bonato, J. U. Hassan, R. Karhu, I.G. Ivanov, N.T. Son, J.R. Maze, T. Ohshima, Ö.O. Soykal,

Á. Gali, S.Y. Lee, F. Kaiser, J. Wrachtrup, Nat. Commun. 10 (2019) 1954, https://doi.org/10.1038/s41467-019-09873-9.
[13] N.T. Son, C.P. Anderson, A. Bourassa, K.C. Miao, C. Babin, M. Widmann, M. Niethammer, J.U. Hassan, N. Morioka, I.G. Ivanov, F. Kaiser, J. Wrachtrup, D. D. Awschalom, Appl. Phys. Lett. 116 (2020) 190501, https://doi.org/10.1063/5.0004454.
[14] Z. Zhou, Z. Xu, Y. Song, C. Shi, K. Zhang, B. Dong, Nanomanufacturing Metrol. (2023) 6, https://doi.org/10.1007/s41871-023-00186-6.
[15] Y.C. Chen, P.S. Salter, M. Niethammer, M. Widmann, F. Kaiser, R. Nagy, N. Morioka, C. Babin, J. Erlekampf, P. Berwian, M.J. Booth, J. Wrachtrup, Nano Lett. 19 (2019) 2377, https://doi.org/10.1021/acs.nanolett.8b05070.
[16] Z. Lin, L. Ji, Y. Wu, L. Hu, T. Yan, Z. Sun, Appl. Surf. Sci. 469 (2019) 68, https://doi.org/10.1016/j.apsusc.2018.11.015.
[17] Z. Lin, L. Ji, T. Yan, Y. Xu, Z. Sun, J. Mater. Res. Technol. 8 (2020) 5934, https://doi.org/10.1016/j.jmrt.2020.03.120.
[18] S. Sato, T. Narahara, Y. Abe, Y. Hijikata, T. Umeda, T. Ohshima, Appl. Phys. 126 (2019), 083105, https://doi.org/10.1063/1.5099327.
[19] T.N. Oder, T.L. Sung, M. Barlow, J.R. Williams, A.C. Ahyi, T. Isaacs-Smith, J. Electron. Mater. 38 (2009) 772, https://doi.org/10.1007/s11664-009-0739-x.
[20] G.R. Yazdi, T. Iakimov, R. Yakimova, Crystals 6 (2016) 53, https://doi.org/10.3390/cryst6050053.
[21] S. Lee, M.F. Toney, W. Ko, J.C. Randel, H.J. Jung, K. Munakata, J. Lu, T.H. Geballe, M.R. Beasley, R. Sinclair, H.C. Manoharan, A. Salleo, ACS Nano 4 (2010) 7524, https://doi.org/10.1021/nn101796e.
[22] M. Hattori, H. Ikenoue, D. Nakamura, K. Furukawa, M. Takamura, H. Hibino, T. Okada, Appl. Phys. Lett. 108 (2016), 093107, https://doi.org/10.1063/1.4943142.
[23] I. Choi, H.Y. Jeong, H. Shin, G. Kang, M. Byun, H. Kim, A.M. Chitu, J.S. Im, R. S. Ruoff, S.Y. Choi, K.J. Lee, Nat. Commun. 30 (2016), 13562, https://doi.org/10.1038/ncomms13562.
[24] G.A. Shafeev, L. Bellard, J.-M. Themlin, C. Fauquet-BenAmmar, A. Cros, W. Marine, Surf. Coating. Technol. 80 (1996) 224, https://doi.org/10.1016/0257-8972(95)02717-3.
[25] P.E. Pehrsson, R. Kaplan, J. Mater. Res. 4 (1989) 1480, https://doi.org/10.1557/JMR.1989.1480.
[26] R. Delmdahl, O. Haupt, B. Berenbak, L. deVreede, A. Janssens, Laser-based Micro- and Nanoprocessing XVI, 2022, https://doi.org/10.1117/12.2606173, 119890K.
[27] J.C. Conde, E. Martín, S. Chiussi, F. Gontad, C. Serra, P. González, Appl. Phys. Lett. 97 (2010), 014102, https://doi.org/10.1063/1.3452341.
[28] M. Diez, M. Ametowobla, T. Graf, J. Laser Micro. Nanoengineering 12 (2017) 230, https://doi.org/10.2961/jlmn.2017.03.0010.
[29] A.P. Menduiña. UV laser processing of SiC and its characterization, MSc thesis, University of Vigo, 2022.
[30] S. de Unamuno, E. Fogarassy, Appl. Surf. Sci. 36 (1989) 1, https://doi.org/10.1016/0169-4332(89)90894-5.
[31] J.C. Conde, E. Martín, F. Gontad, S. Chiussi, L. Fornarini, B. León, Thin Solid Films 518 (2010) 2431, https://doi.org/10.1016/j.tsf.2009.09.135.
[32] M.A. Green, Sol. Energy Mater. Sol. Cells 92 (2008) 1305, https://doi.org/10.1016/j.solmat.2008.06.009.
[33] J. Solis, C.N. Afonso, J. Appl. Phys. 69 (1991) 2105, https://doi.org/10.1063/1.348968.
[34] J. Boneberg, O. Yavas, B. Mierswa, P. Leiderer, Phys. Status Solidi 174 (1992) 295, https://doi.org/10.1002/pssb.2221740130.
[35] S. Nakashima, H. Harima, Phys. Status Solidi 162 (1997) 39, https://doi.org/10.1002/1521-396X(199707)162:1<39::AID-PSSA39>3.0.CO;2-L.
[36] H. Harima, Microelectron. Eng. 83 (2006) 126, https://doi.org/10.1016/j.mee.2005.10.037.
[37] T. Kimoto, J.A. Cooper, e-ISBN 9781118313534 (Chapter 5).1.2, John Wiley & Sons Singapore Pte. Ltd Singapore, 2014, https://doi.org/10.1002/9781118313534.
[38] S.A. Kukushkin, A.V. Osipov, J. Appl. Phys. D: Appl. Phys. 47 (2014), 313001, https://doi.org/10.1088/0022-3727/47/31/313001.
[39] A. Kole, P. Chaudhuri, AIP Adv. 4 (2014), 107106, https://doi.org/10.1063/1.4897378.
[40] V.A. Volodin, D.I. Koshelev, J. Raman Spectrosc. 444 (2013) 1760, https://doi.org/10.1002/jrs.4408.
[41] F. Gontad, J.C. Conde, S. Filonovich, M.F. Cerqueira, P. Alpuim, S. Chiussi, Thin Solid Films 536 (2013) 147, https://doi.org/10.1016/j.tsf.2013.04.005.
[42] Ch Ossadnik, S. Veprek, I. Gregora, Thin Solid Films 337 (1999) 148, https://doi.org/10.1016/S0040-6090(98)01175-4.
[43] A.C. Ferrari, Solid State Commun. 143 (2007) 47, https://doi.org/10.1016/j.ssc.2007.03.052.
[44] Z.H. Ni, W. Chen, X.F. Fan, J.L. Kuo, T. Yu, A.T.S. Wee, Z.X. Shen, Phys. Rev. B 77 (2008), 115416, https://doi.org/10.1103/PhysRevB.77.115416.
[45] L.M. Malard, M.A. Pimenta, G. Dresselhaus, M.S. Dresselhaus, Phys. Rep. 472 (2009) 51, https://doi.org/10.1016/j.physrep.2009.02.003.
[46] J.B. Wu, M.L. Lin, X. Cong, H.N. Liu, P.H. Tan, Chem. Soc. Rev. 47 (2018) 1822, https://doi.org/10.1039/c6cs00915h.